

1 **Supplementary documents**

2 **S1 The comparison between the sub-model approach and Arc-Malstrøm**

3 The program of the sub-model approach is adapted from the prototype of Arc-Malstrøm. To clarify their
4 distinctions, which in turn demonstrates the novelty of this approach, we compare the sub-model approach to
5 Arc-Malstrøm on the level of theory, input and output (Table S1a). Firstly, as opposed to Arc-Malstrøm's 1D
6 static flow, the sub-model approach uses MIKE FLOOD's 2D dynamic flows (Phase II) to obtain final flood
7 predictions, while 1D static flows (Phase I) are exclusively used for identifying reduced domains as well as
8 optimised boundaries for faster 2D flow computations. As such, unlike Arc-Malstrøm's single time simulation,
9 the sub-model approach illustrates a multiple simulation process, involving different routings (1D static/ 2D
10 dynamic flows) considering different modelling complexities (see Table S1a) at multiple scales (basin/local
11 catchment scale), which improves the holistic modelling performance. Secondly, whereas high-resolution
12 DEMs are required by both approaches, differences come at rainfall datasets. Arc-Malstrøm simply demands
13 a value of the total rainfall amount reflecting a uniform static rainfall, whereby $\text{Catchment Area} \times \text{Rain Amount}$
14 is used for the calculation of runoff volumes. In contrast, 2D rainfalls datasets, that incorporates rainfall spatial
15 variations and time evolutions in the form of Time-series raster, are required by the sub-model approach. Here,
16 Eq. (2) is used for the runoff computation of the distributed static rainfall in Phase I, while MIKE FLOOD's
17 2D solver accounts for a distributed dynamic rainfall in Phase II. Lastly, for the sake of distinctions above,
18 differences in outputs are identified as well. Arc-Malstrøm's primary outputs illustrate final flood volumes
19 (i.e. spill-over volumes and % filled volumes) distribution maps, and its flood extent (so-called "blue spot
20 maps") are exclusively based on sinks' extents. However, based on MIKE FLOOD's 2D simulations, the sub-
21 model approach's final outputs illustrate dynamic 2D predictions on flood extents, depths and flow velocities
22 within each grid-cell of high-resolution DEMs, which deliver more precise flood information as opposed to
23 Arc-Malstrøm.

24 In addition, to clarify further developments, module-to-module comparisons regarding the two approaches'
25 algorithms are presented in Table S1b. Here, four major improvements are summarised: i) the sink screening

26 method (VRSS) was proposed to determine computationally important sinks and their volumes for accurate
27 network generations and its subsequent computations; ii) the link-based fast-inundation algorithm was
28 programmed exclusively based on stream links feature class to estimate full-basin 1D flow conditions, and a
29 simple data structure was self-established to assemble all computational information within one attribute table;
30 iii) an iterative search procedure was developed to trace sub-impact zones relevant to target object, where the
31 self-identified connectivity and a Boolean flow condition property was used to determine optimal tracing
32 distances; iv) the effect of basin-wise rainfall heterogeneity was addressed in i) and ii) by integrating Eq. (2).

33 Generally, substantial differences have been identified in terms of theory, inputs, outputs and algorithms used.
34 Thus, we conclude that Arc-Malstrøm and the sub-model approach are two different applications. Furthermore,
35 we extended two comparison tests regarding the network generation in Supplementary Document S2 and the
36 flood extent prediction in Supplementary Document S3.

37
38
39
40
41
42
43
44
45
46
47
48
49
50
51

52

53 **Table S1a**

54 The theory, input and output comparison between the sub-model approach and Arc-Malstrøm.

		Sub-model approach	Arc-Malstrøm
Theory	Routings	<ul style="list-style-type: none"> Phase I: 1D static flows (basin scale); Phase II: 2D dynamic flows (local catchment scale). 	<ul style="list-style-type: none"> 1D static flows.
	Modelling complexities	<ul style="list-style-type: none"> Phase I considers the inundation process only. Thus, hydrological losses nor drainage volumes are neglected; Phase II allows for the inclusion of more modelling complexities (i.e. infiltrations, evapotranspiration and distributed roughness) within each computational cell during MIKE FLOOD 2D simulations. 	<ul style="list-style-type: none"> Arc-Malstrøm considers infiltration as volume losses (Hortonian flow) for each sink's mass balance conservation. The drainage system is not considered.
	Speed-up mechanisms	<ul style="list-style-type: none"> Computational domain reductions for 2D flow computations; Multiple simulations involving different modelling complexities at different scales to gain holistic computational efficiency. 	<ul style="list-style-type: none"> Simplified routing exclusively governed by the conservation of mass balance.
Inputs		<ul style="list-style-type: none"> High-resolution DEMs (DHyM + DSM); Distributed 2D rainfalls with the time evolution: distributed static rainfall (Phase I, computed by Eq. (2)) + distributed dynamic rainfall (Phase II, computed by MIKE FLOOD); Target objects. 	<ul style="list-style-type: none"> High-resolution DEM (DHyM); Static uniform rainfall (total rainfall amount), computed by Catchment Area \times Rain Amount; Distributed subsurface map accounting for distributed infiltration process.
Outputs	Types	<ul style="list-style-type: none"> Dynamic 2D predictions. 	<ul style="list-style-type: none"> Static 1D predictions.
	Flood extents	<ul style="list-style-type: none"> Flood extents based on maximum flood depths. 	<ul style="list-style-type: none"> Flood extents based on sink extents (blue spots map).
	Flood depths	<ul style="list-style-type: none"> Maximum flood depths summarised from dynamic flood depths based on each grid-cell, thus capturing peak flood precisely. 	<ul style="list-style-type: none"> No flood depth provided; Instead, final flood volumes within each sink (i.e. spill-over volumes and % filled volumes) are provided.
	Flow velocity	<ul style="list-style-type: none"> Flow velocities provided in u- and v-directions based on each grid-cell. 	<ul style="list-style-type: none"> No flow velocity provided.

55

56

57

58

59

60

61

62

63

64 **Table S1b**

65 Module-to-module comparison table between the sub-model approach and Arc-Malstrøm.

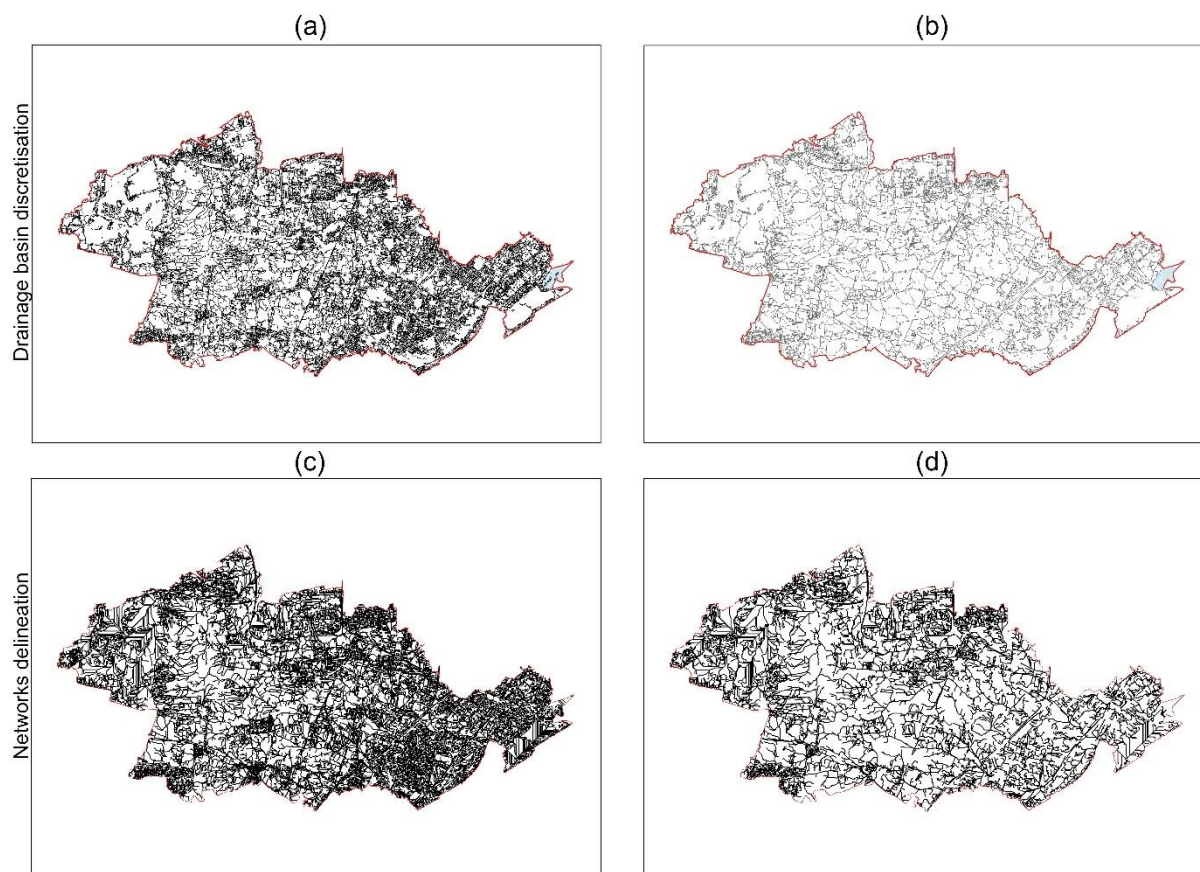
		Sub-model approach	Arc-Malstrøm
Algorithms distinction for each module	Sink screening (Module I)	<ul style="list-style-type: none"> • Volume Ratio Sink Screening. 	<ul style="list-style-type: none"> • Sink screening criterion based on sink's maximum depth, where sinks less than DEMs' vertical accuracy (i.e. 0.05m) are eliminated.
	Network generation (Module II)	<ul style="list-style-type: none"> • The network without using the ArcGIS' geometric network data structure. 	<ul style="list-style-type: none"> • Using ArcGIS' geometric network to assemble networks.
	Fast-inundation spreading algorithm (Module III)	<ul style="list-style-type: none"> • Computation has independency to ArcGIS' geometric network; • Programming in Python; • Computational information coded on Stream Link feature class; • Computing order determined by Shreve order; • Topological connectivity self-identified by ArcGIS' Spatial Join tool; • Computational information and topological connectivity configured in one table. 	<ul style="list-style-type: none"> • Computation based on ArcGIS' geometric network; • Programming in C# under .Net framework via ArcObject SDK; • Computational information coded on the geometric network's points class; • Computing order determined by accessing point-to-point relation from the geometric network's relation class; • Topological connectivity established by assessing the geometric network's functions. • Computational information and topological connectivity stored in separate class objects in the geometric network.
	Search algorithm (Module IV)	<ul style="list-style-type: none"> • Upstream tracing based on the self-identified topological connectivity; • Tracing distance determined by considering spill-over /non-spill-over as a termination criterion for the searching loop. 	<ul style="list-style-type: none"> • Upstream tracing provided based on the geometric network's function; • Tracing distance determined from topological connectivity only.
	2D flow computations (Module V)	<ul style="list-style-type: none"> • 2D flow computations based on MIKE FLOOD by using reduced domains and optimised boundary conditions. 	×

66

67 **S2 Comparison tests of network generations between Arc-Malstrøm and the sub-model approach.**

68 To distinct networks generated by Arc-Malstrøm and the sub-model approach, by adopting the vertical
69 accuracy of 0.05 m and HRV_{ratio} of 15 % as sink screening criteria, different networks were configured based
70 on the corresponding sink configurations. These networks' spatial layouts were investigated from two
71 perspectives: drainage basin discretisation (Fig. S2 a and b) and network delineations (Fig. S2 c and d).
72 Besides, their geometric properties were summarised based on geometric statistic in Table S2.

73 In contrast to Arc-Malstrøm, the sub-model approach shows intuitively simpler drainage basin discretization
74 (Fig. S2 a and b). In Table S2, substantially larger average areas of 7555 m² and the smaller number of 9703
75 were observed for discretised sub-impact zones of the sub-model approach. Also, a simpler network
76 complexity was identified for the sub-model approach compared to Arc-Malstrøm, and the smaller network
77 density of 0.0153 m⁻¹ and the smaller number of links (13,559) were obtained. Due to the decreased number
78 of the 1st and 2nd order links, the reduced Max. Shreve order of 6611 was found for the sub-model approach's
79 network. Yet, highly densified networks were found in the northern and western parts of the Greve basin (Fig.
80 S2 d), which is in accordance with basin-wise rainfall distributions of Thiessen polygons (Fig. 9). Here, more
81 sinks were preserved in these regions hit by smaller rainfalls, configuring more detailed networks to improve
82 the 1D surface runoff representations.



83
84 Fig. S2 Network generation comparisons between Arc-Malstrøm and the sub-model approach: (a) Arc-Malstrøm's drainage basin
85 discretisation, (b) Sub-model approach's drainage basin discretisation, (c) Arc-Malstrøm's network delineations and (d) Sub-model
86 approach's network delineations.

87

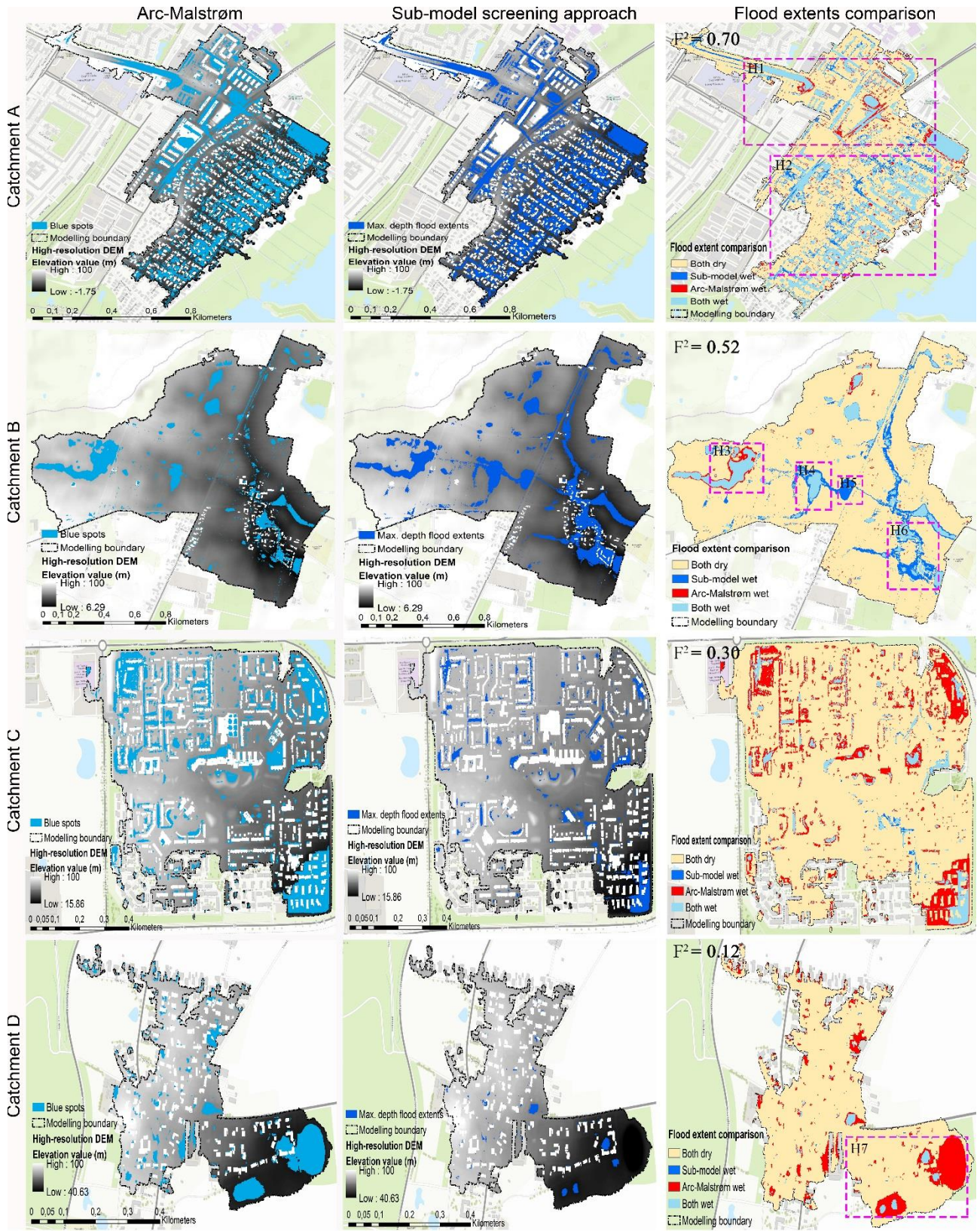
88 Table S2 Geometric statistic for network generated by Arc-Malstrøm and the sub-model approach.

		Arc-Malstrøm's network	Sub-model approach's network	
Drainage basin discretisation	No. of sub-impact zones	38131	9703	
	Average areas of sub-impact zones (m ²)	1925	7555	
Network delineation	Network density (m ⁻¹)	0.0267	0.0153	
	Total length (m)	1990314	1130862	
	Average length of links (m)	52 m	83	
	Links No.	38554	13559	
	Max. Shreve order	18620	6611	
	1 st order links	Average length (m)	53	86
		Link No.	19479	6849
	2 nd order links	Average length (m)	51	82
Link No.		4840	1708	

89 Note: Network density = Total length of networks / Total drainage basin areas, which reflects the network concentration in each
90 drainage area.

91 **S3 Prediction results comparison tests between Arc-Malstrøm and the sub-model approach.**

92 According to Table S1, flood extents were identified as the joint output for Arc-Malstrøm and the sub-model
93 approach. To further distinguish their prediction discrepancies, cell-by-cell comparisons of the two approaches
94 were conducted by using the binary analysis (dry /wet) considering four different catchment areas as well as
95 different rainfall return periods (1-100 year), see Fig. S3. In catchment A, a goodness of fit ($F^2 = 0.7$) between
96 the two approaches was observed, especially for the downstream areas (H2) hit by extreme rainfalls of 98.6
97 mm. However, underestimations (blue cells), distributing along the flow paths, were found for Arc-Malstrøm.
98 In accordance with findings by Jahanbazi and Egger, (2014) and Jamali et al., (2018), Arc-Malstrøm (as a
99 static model) cannot provide flood predictions beyond the location of sinks and, therefore, the flow conditions
100 along pathways may be miss-captured. In addition, due to the different approaches to defining flood extents,
101 the sub-model approach, delineating flood extents based on flood depths of each grid-cell, may exclude the
102 flooded cells of < 10 cm inside sinks, thus resulting in discrepancies, e.g. red cells in H1 and H3. In catchment
103 B, significant underestimations were spotted in H4 and H6 when using Arc-Malstrøm. Due to the special
104 catchment topologies, substantially converged flow accumulations may deliver high-momentum flows
105 throughout long propagation paths, thus reaching more areas (blue cells) beyond sink extents (light blue cells).
106 Notable miss-predictions were identified for Arc-Malstrøm in H5. Here, the occurrence of the water ponding
107 was ascribed to the limited discharge of the downstream highway underpass, and such flood peaks can be
108 captured, only, during dynamic simulations. In catchments C and D, significant discrepancies of $F^2 = 0.30$ and
109 0.12 were suggested for the comparison of the two approaches. Because non-spill-over sinks present much
110 smaller inundation extents than sink's full extents, Arc-Malstrøm overestimated flood extents substantially in
111 case of small rainfall events. Whereas identifying a volume-depth curve for each sink may suggest more precise
112 flood extents (Jamali et al., 2018, Zhang and Pan, 2014), it is quite challenging to identify realistic flood extents
113 for those sinks comprising several small sinks, e.g. the sink on the right side of H7, and its small sinks to the
114 left were filled first.



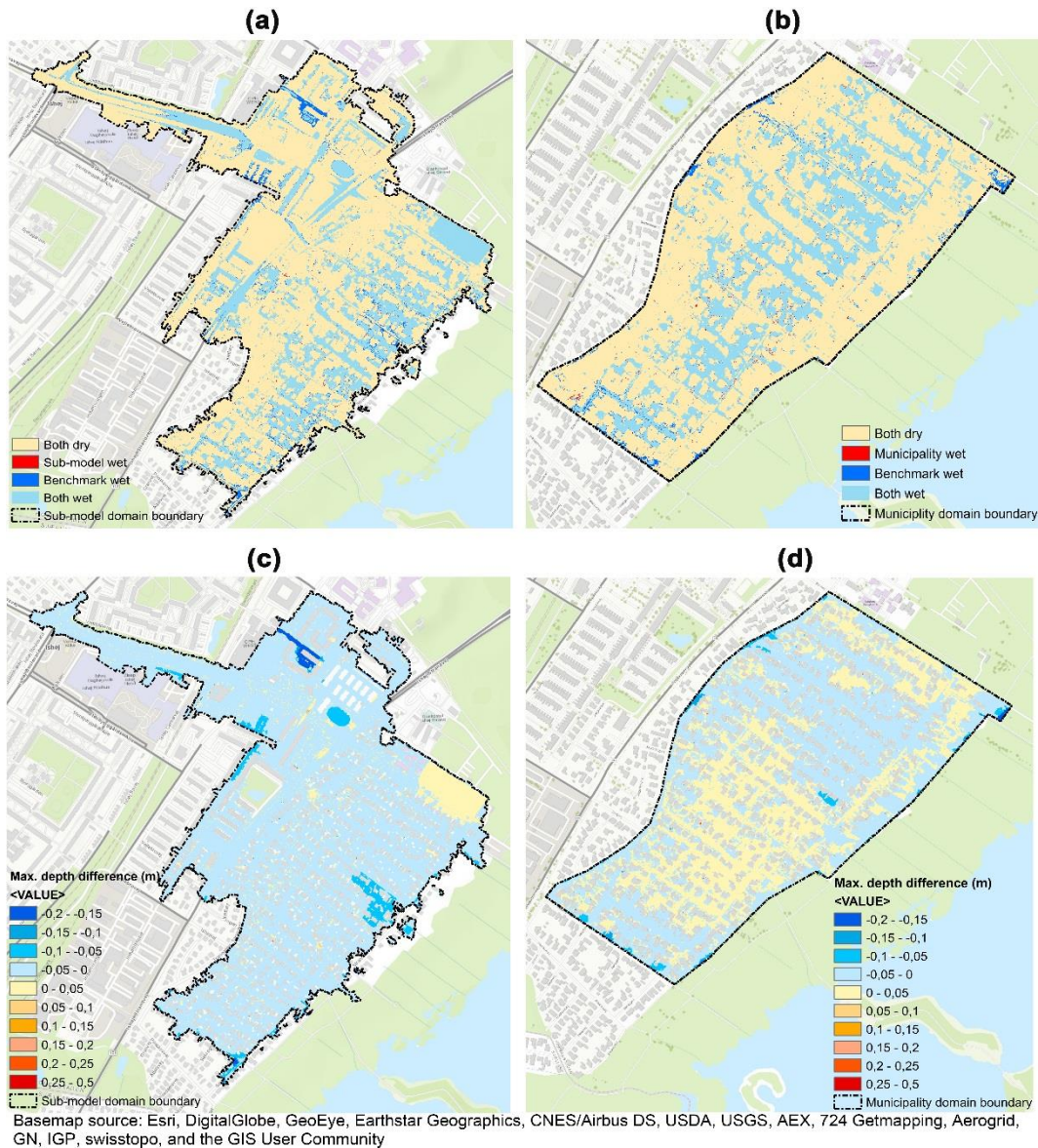
116
 117
 118
 119
 120
 121

Basemap source: Esri, DigitalGlobe, GeoEye, Earthstar Geographics, CNES/Airbus DS, USDA, USGS, AEX, 724 Getmapping, Aergrid, IGN, IGP, swisstopo, and the GIS User Community

Fig. S3 Flood extent comparisons between Arc-Malstrøm and the sub-model approach based on four catchments area representing different terrain morphologies as well as different rainfall return periods (1-100 year), where the first column represents the Arc-Malstrøm's flood extent predictions, the second column represent the sub-model approach's flood extent predictions, and the third column is categorised maps showing the discrepancies in flood extent predictions.

122 **S4 Comparison tests using the uniform open-boundary condition.**

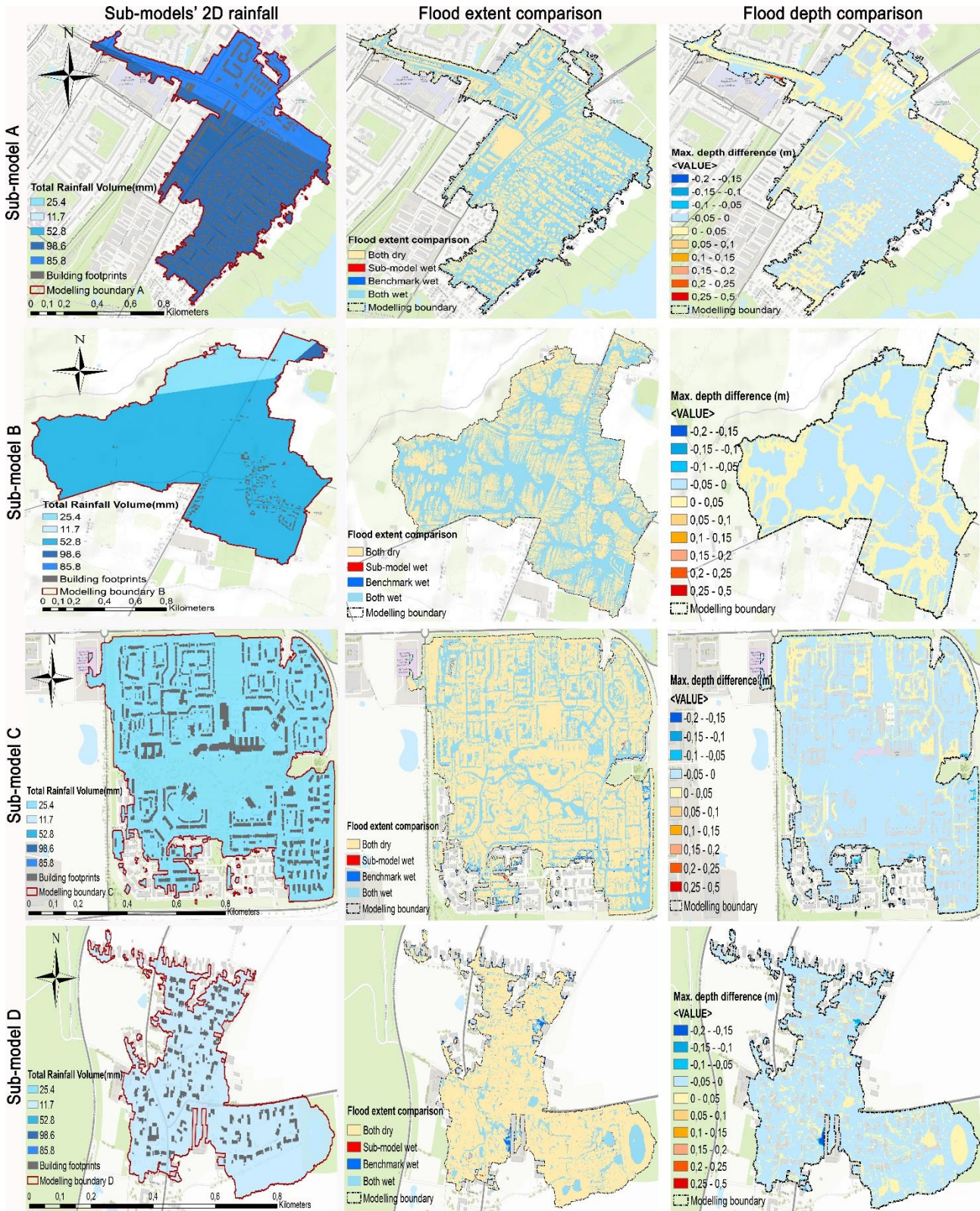
123 The comparison test using the uniform open-boundary condition are presented from the perspective of
124 maximum flood extents (Fig. S4a and b) and maximum flood depths (Fig. S4 c and d). Significant
125 underestimations in maximum flood extents and maximum flood depths were seen for the two approaches.
126 Due to the massive leakages of runoff volumes via the open-boundary conditions, the 2D runoffs, which were
127 supposed to accumulate locally and then flowed into the central area, escaped directly from their closest edges.
128 These hydraulic behaviours violated the 1D flow pattern pre-defined, thus these results were recognised as
129 miss-predictions and must not be used for domain reduction tests.



130 Fig. S4 Maximum depth flood extents and maximum depth differences with the uniform open-boundary condition: (a) Sub-model
131 approach's categorised map, (b) Municipality domain approach's categorised map, (c) Sub-model approach's depth difference map,
132
133 (d) Municipality domain approach's depth difference map.

134
135

S5 Extracted 2D rainfalls for four sub-models and comparison maps for four sub-model predictions



136
137
138
139

Basemap source: Esri, DigitalGlobe, GeoEye, Earthstar Geographics, CNES/Airbus DS, USDA, USGS, AEX, 724 Getmapping, Aerogrid, IGN, IGP, swisstopo, and the GIS User Community
 Fig. S5 The first column represents the reduced 2D rainfalls associated with different data volumes in .dfs2 file (MIKE FLOOD 2D's input file format); the second column represents maximum depth flood extent's categorised maps for four sub-models and the third column represents maximum depth's depth difference map for four sub-models.